ORIGINAL RESEARCH

Comparison of image georeferencing strategies for agricultural applications of small unoccupied aircraft systems

N. Ace Pugh[1] | **Kelly R. Thorp**[2] | **Emmanuel M. Gonzalez**[1] |
Diaa Eldin M. Elshikha[3,4] | **Duke Pauli**[1]

[1] School of Plant Sciences, Univ. of Arizona, Tucson, AZ 85721, USA

[2] USDA-ARS, U.S. Arid-Land Agricultural Research Center, Maricopa, AZ 85138, USA

[3] Biosystems Engineering, Univ. of Arizona, Tucson, AZ 85721, USA

[4] Agricultural Engineering Dept., Faculty of Agriculture, Mansoura Univ., Al Mansoura, Egypt

Correspondence
Duke Pauli, School of Plant Sciences, Univ. of Arizona, Tucson, AZ 85721, USA.
Email: dukepauli@arizona.edu

Assigned to Associate Editor Daniel Northrup.

Abstract

Small unoccupied aircraft systems (sUAS) are becoming popular for mapping applications in agriculture, and photogrammetry software is available for developing orthorectified imagery and three-dimensional surface models. Ground control points (GCPs), which are objects or locations with known geographic coordinates, may be required for accurate image georeferencing. However, few studies have compared global position equipment among sUAS or investigated the effects of GCP number or arrangement on georeferencing accuracy. The objectives of this study were to evaluate numbers and configurations of GCPs for georeferencing sUAS-acquired images and determine the GCP requirements for sUAS with and without real-time kinematic (RTK) global positioning equipment. The effects of varying numbers and configurations of GCPs were investigated on both a 0.40-ha area the size of a typical plant breeding trial and a 64.7-ha area (i.e., a U.S. quarter section) the size of a typical agricultural production field. Results demonstrated that four GCPs placed at the corners of the breeding-scale field resulted in two-dimensional (2D) error of ±3 cm in the absence of RTK, with minimal improvements when including more GCPs. The orthomosaics from the RTK-equipped sUAS demonstrated improved 2D accuracy even without the use of GCPs, with a maximum mean error of 0.08 m. Four GCPs were found to be sufficient to reduce altitudinal (Z) error, with maximum mean error of only 0.05 and 1.98 m for the RTK and non-RTK flights, respectively, for the production-scale field. Thus, using four GCPs, RTK-equipped sUAS, or a combination will result in improved georeferencing for photogrammetry products.

1 | INTRODUCTION

Remote sensing technologies are useful for agricultural research scientists to map their experimental trials (Anderson et al., 2019; Araus & Cairns, 2014; Gracia-Romero et al., 2019; Pauli, Andrade-Sanchez et al., 2016; Shi et al., 2016). Small unoccupied aircraft systems (sUAS) are a novel

Abbreviations: DEM, digital elevation map; DSM, digital surface map; GCP, ground control point; GNSS, global navigation satellite system; GPS, global positioning system; ODM, OpenDroneMap; P4PRO, Phantom 4 Pro; P4RTK, Phantom 4 RTK; RGB, red-green-blue; RTK, real-time kinematic; SfM, structure from motion; sUAS, small unoccupied aircraft systems; UTM, universal transverse mercator.

technology for high-throughput plant phenotyping, which is the fast and accurate measurement of plant morphology and properties (Li et al., 2020; Malambo et al., 2018; Pauli, Chapman et al., 2016; Sankaran et al., 2015; Singh et al., 2019; Xie & Yang, 2020). Small unoccupied aircraft system platforms have been used in numerous agricultural studies, implemented in plant breeding programs, and applied in a multitude of economically important crops worldwide including maize (*Zea mays* L.), sorghum [*Sorghum bicolor* (L.) Moench], cotton (*Gossypium hirsutum* L.), rice (*Oryza sativa* L.), and wheat (*Triticum aestivum* L.) (Anderson et al., 2019; Gracia-Romero et al., 2019; Pugh et al., 2018; Yeom et al., 2018; Zhou et al., 2017). Rotary-wing sUAS, such as quad or hexacopters, equipped with red-green-blue (RGB) cameras were deployed for many of these studies, because they are relatively simple to use in field-based, agricultural research.

Orthomosaics generated from sUAS-based RGB imagery can be used to delineate plants or plot boundaries and to compute vegetation indices. Three-dimensional (3D) structural details can also be derived from digital surface maps (DSMs) created using structure from motion (SfM), a process by which 3D surfaces are reconstructed from a point cloud created by imaging the scene from multiple angles (Schonberger & Frahm, 2016; Westoby et al., 2012). These photogrammetry techniques are important for quantifying phenotypic variation in structural plant characteristics, such as plant height and canopy cover, which are traits that estimate plant growth and development during a growing season. However, the geospatial accuracy of photogrammetric products and ultimately plant phenotyping results requires proper georeferencing of the sUAS image data. The need for high geospatial precision and accuracy can be addressed using standard tools in aerial photogrammetry such as ground control points (GCPs) as well as newer technologies, such as sUAS, that incorporate real-time kinematic (RTK)-global positioning system (GPS) equipment (Ekaso et al., 2020; Przybilla et al., 2020). However, few studies have investigated the use of these techniques in tandem and for agricultural applications, specifically.

Ground control points are physical objects or locations for which accurate geographic coordinates are known; they serve to anchor photogrammetric products to a known, physical coordinate system (Colomina & Molina, 2014; Rabah et al., 2018; Westoby et al., 2012). By using GCPs for which the accurate and precise coordinates are known a priori, subsequent processing and resulting orthomosaics and DSMs can be properly georeferenced using a process known as aerial triangulation (Rabah et al., 2018; Westoby et al., 2012). This is crucial when the exact spatial relationship between objects and centimeter-level accuracy is required, as is frequently the case when image datasets must be compared with other spatial data sources or when multiple image sets must be compared over time. This level of accuracy is particularly important in studies conducted by plant

Core Ideas

- Four ground control points are sufficient to georeference aerial photogrammetry projects.
- Real-time kinematic positioning data can be used instead of ground control points (GCPs) to georeference projects.
- Using GCPs and real-time kinematic positioning together results in highly accurate products.
- Popular photogrammetry software perform similarly and can each be used for agriculture.

breeders to elucidate specific phenotypes in their chosen crop or crops; however, many sUAS incorporate GPS that only achieves meter-level accuracy and may not be suitable for this purpose (Borra-Serrano et al., 2020; Kawamura et al., 2020; Su et al., 2019). To obtain centimeter-level accuracy in georeferencing scenarios, sUAS must be able to geotag objects and locations correctly. As noted previously, sUAS equipped with RTK-GPS technology are becoming an option for sUAS pilots; however, there has not been rigorous study into their efficacy when used for plant breeding and agricultural production applications.

Although GCPs are simple to implement and efficient to use, they are nonetheless a primary bottleneck in photogrammetry processing pipelines (Colomina & Molina, 2014; Forlani et al., 2019). The choice of GCP material is often dictated by its identifiability in images, how easy they are to place in the field, and how obstructive they are to field operations (Forlani et al., 2019). Although it is now widely understood that multiple GCPs are required to properly georeference imagery collected with sUAS, the number and configuration of GCPs that are necessary to obtain accurate results is less clear and must also be balanced with the time required for manual GCP installation and incorporation of those GCP data into photogrammetry pipelines (Villanueva & Blanco, 2019; Wang et al., 2012). Indeed, the number and placement of GCPs that have been used by researchers in photogrammetry studies vary widely, even within the same crop species. For example, in a study conducted in cotton by Thorp et al. (2018), 21 GCPs were identified from static features around a six-hectare study area, whereas in another cotton study by Huang et al. (2016), four GCPs were used to cover each of the 0.6-ha study areas (Huang et al., 2016; Thorp et al., 2018). Though the usage of GCPs for georeferencing sUAS imagery is commonplace, there are few studies that have investigated the effects of GCP number and configuration on the georeferencing accuracy of photogrammetry products, and with respect to agricultural and plant science research, even fewer (Agüera-Vega et al., 2017; Martínez-Carricondo et al., 2018; Ren et al., 2020;

Sanz-Ablanedo et al., 2018; Tonkin & Midgley, 2016; Villanueva & Blanco, 2019; Zimmerman et al., 2020).

Ground control points have been used for image georeferencing for several decades, but sUAS capable of geotagging using RTK-GPS, such as the DJI Phantom 4 RTK, have only recently become available (Forlani et al., 2019; Taddia et al., 2019). These RTK-equipped sUAS incorporate a stationary global navigation satellite system (GNSS) receiver (i.e., base station), which is used to correct positions measured with the rover GNSS receiver aboard the sUAS. Because the precise knowledge of the stationary receiver is incorporated into the triangulation calculations of the location of the roving receiver, centimeter-level accuracy can be achieved and applied to the geotagging of images (Fazeli et al., 2016; Forlani et al., 2018, 2019; Obanawa et al., 2019). Due to this high level of geospatial accuracy, RTK-equipped sUAS may permit collection of image data without the need for GCPs (Rabah et al., 2018). More studies comparing the efficacy of sUAS platforms with and without RTK technology are needed to determine how well RTK technology performs, and the effect of using RTK in tandem with GCPs is also important to evaluate.

It is important to consider that sUAS merely assign coordinates to image frames during data collection and the use of photogrammetry software is required to process those image frames. It is therefore exceedingly difficult to obtain data that are useful for phenotyping applications from photogrammetric products that do not use some external method to georeference the images, either via GCPs or RTK positioning. These photogrammetry programs use geotagged images to develop sparse point clouds, and dense point clouds are developed using SfM (Schonberger & Frahm, 2016; Westoby et al., 2012). From the orthomosaics produced by this processing, researchers and producers can extract useful phenotypes for their crop of choice. There are several choices of photogrammetry software available for these sUAS applications, ranging from free and open-source software to proprietary, commercial software. Although researchers have many potential options, a detailed comparison of the capabilities of each software are necessary to identify differences in georeferenced orthomosaics arising from choice of software.

The conventional wisdom for many agricultural researchers has been to use as many GCPs as time and funding allows to attempt to maximize the potential accuracy of photogrammetry products; however, few studies have investigated GCP usage and determined when accuracy thresholds are reached. In addition, RTK technology has not yet been evaluated for its use when implementing aerial photogrammetry techniques in plant breeding programs or in agricultural production. To address these needs, we sought to determine what the optimal GCP number and configuration for different field scales is and whether RTK technology could supplement or even replace GCPs as a georeferencing method in the future. It was also crucial that several popular photogrammetry software programs be evaluated and compared for the accuracy of their products and ability to use those products to extract potential phenotypes. To assess the impact of using different GCP configurations and RTK technology and identify the best practices for georeferencing sUAS imagery of agricultural fields, as well as the differences in the processed imagery between three popular photogrammetry applications, the objectives of this study were (a) to determine the most effective number and configuration of GCPs for aerial photogrammetry from sUAS, (b) to determine the effectiveness of RTK-equipped sUAS platforms when compared with non-RTK sUAS, and (c) to compare the georeferencing accuracy of current photogrammetry software.

2 | MATERIALS AND METHODS

2.1 | Field site

The experiment used two field areas located at the Maricopa Agricultural Center in Maricopa, AZ. The first field area was 0.4-ha, centered on the coordinates of 408242.279, 3661040.007 (WGS84/universal transverse mercator [UTM] Zone 12N) and representative of typical plant breeding trials ("breeding-scale field", Figure 1a). A total of 63 ground control points (GCPs) were arranged in a staggered grid pattern with nine rows consisting of seven GCPs with each row offset from the adjacent row(s) (Figure 1a). The spacing between GCPs from east to west and from north to south was approximately 7.6 m, and each alternating row had an offset of approximately 3.8 m. The second field area was 64.7-ha, a U.S. quarter-section, centered on the coordinates of 408388.680, 3661075.562 (WGS84/UTM Zone 12N) and representative of a production-scale agricultural field ("production-scale field," Figure 1b). A total of 25 GCPs were placed in a grid pattern with five rows and five GCPs in each row. The spacing between GCPs from east to west was approximately 188 m, while the spacing from north to south was approximately 196 m. Preliminary coordinate locations of the 25 GCPs were identified using a digital orthophoto quadrangle of the field area, and an RTK-enabled rover was used to navigate the field area for GCP placement. The breeding-scale field area was located within the boundaries of the production-scale field area, but the two field areas did not share any GCPs in common. Both fields were fallow throughout the entire study, and a chisel plow had been used to eliminate weeds prior to the collection of imagery.

White plastic bucket lids (Uline Inc.) with a diameter of 31 cm were used as the GCPs in both field areas, secured by 30.5-cm metal stakes. To aid in subsequent GCP identification in photogrammetric software, black crosshairs were spray painted on each of the GCPs using a stencil, and they
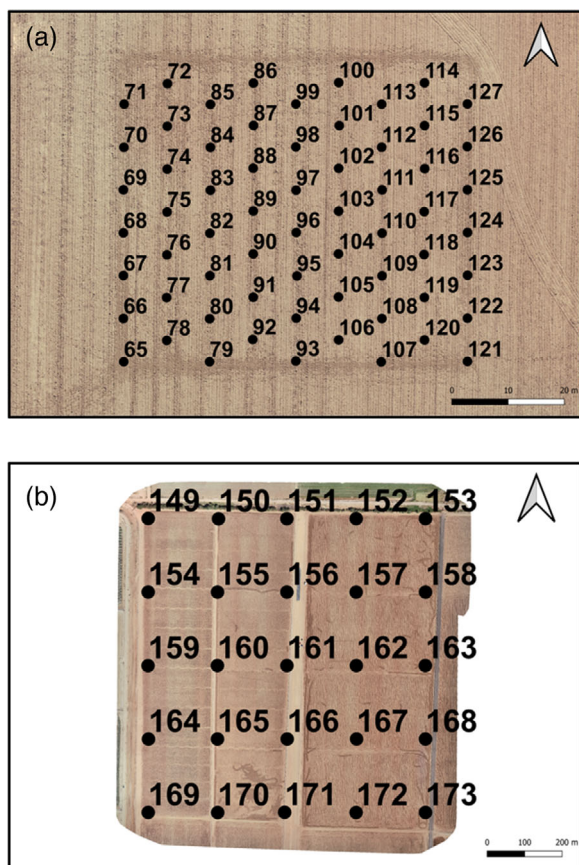
FIGURE 1   Field areas and ground control point (GCP) placement. Layout of GCPs in the 0.4-ha, breeding-scale field area (a) and the 64.7-ha production-scale field area (i.e., a U.S. quarter section) (b). Black markers represent the location of each GCP with numbers representing the GCP identifier

were labeled with an industrial black marker before being placed in their respective positions. The range of numbers marked on the GCPs were 65–127 for the breeding-scale field, and 149–173 for the production-scale field (Figure 1). After placing all the GCPs in both field areas, geographic coordinates (WGS84/UTM Zone 12N) were measured at the center of each GCP using an RTK-GPS instrument (Model #5800, Trimble Inc.).

2.2 | Flight planning and image acquisition

Flight missions were conducted over the field areas using a DJI Phantom 4 RTK (P4RTK; DJI) and a DJI Phantom 4 Pro v.2 (P4PRO; DJI) (Table 1). For the flights conducted with the P4PRO, Pix4Dcapture software (Pix4D, Version 4.12.1) installed on an Apple iPad Mini 4 (Model #MK9P2LL/A; Apple,) was used to conduct the flight missions. The P4RTK flights used the onboard mission control software as provided with the sUAS, and two configurations were tested: with RTK GPS activated (RTK enabled) and with RTK GPS deacti-

vated (RTK disabled). The initial flights of the breeding-scale field and the production-scale field were conducted from 16 Oct. to 18 Nov. 2019 (Table 1). An additional set of flights of the breeding-scale field were also performed on 19 Jan. 2020 to provide a validation dataset using the P4RTK with RTK enabled and RTK disabled (Table 1). All flights of the breeding-scale field using both sUAS platforms were conducted at six different altitudes above ground level (AGL): 25, 40, 60, 80, 100, and 120 m. An AGL of 25 m was the lowest flight altitude permitted by the P4RTK flight control software, and 120 m AGL was the maximum flight altitude permitted by U.S. Federal Aviation Administration (FAA) regulations. To ensure that photogrammetry software could accurately process the images, the front and side image overlap was set at 80%. For the production-scale field, flights were conducted with the P4PRO and the P4RTK with RTK enabled at altitudes of 80, 100, and 120 m AGL, with side and front image overlaps set at 80%. Flights were conducted during an operational window spanning 3 h before and after solar noon on cloud-free days to minimize solar zenith angle, maximize illumination, and minimize shadowing.

2.3 | GCP configurations

A variety of GCP configurations were tested during image processing to identify the optimum number and placement of GCPs for each field area. The configurations and numbers of GCPs that were chosen for this study were based on several potential scenarios and were an attempt to capture the minimum level of effective GCP coverage and the threshold at which improvement in accuracy ceased. Several scenarios were tested, including placing many GCPs in each area to simulate heavy GCP coverage, various configurations of four or five GCPs, one GCP in the center or corner of the field, and zero GCPs. The purpose of placing zero GCPs was to determine how effective RTK technology was for georeferencing alone, and the purpose of placing one GCP was to determine if the product gained any benefit from the inclusion of a single GCP or if it was ineffective or detrimental for georeferencing imagery. In total, eight GCP configurations were tested for the breeding-scale field: (a) no GCPs; (b) one GCP placed in the southwest corner of the field (GCP 65); (c) one GCP placed in the center of the field (96); (d) four GCPs placed at the corners of the field (65, 71, 121, and 127); (e) four GCPs placed at the corners and one placed at the center (65, 71, 121, 127, and 96); (f) four GCPs placed in a box shape nearer to the center of the field (89, 90, 103, and 104); (g) nine GCPs spread evenly across the trial (65, 68, 71, 93, 96, 99, 121, 124, and 127); and (h) the entire set of 63 GCPs (65–127) (Figure 2).

For the production-scale field, six GCP configurations were tested: (a) no GCPs; (b) one GCP placed at the southwest corner of the field (169); (c) one center GCP (161); (d) four

TABLE 1 Flight mission parameters

sUAS	Field	RTK	Altitude	No. of images	Flight date
P4PRO	Breeding-scale	N/A	25	374	18 Nov. 2019
P4PRO	Breeding-scale	N/A	40	146	18 Nov. 2019
P4PRO	Breeding-scale	N/A	60	78	18 Nov. 2019
P4PRO	Breeding-scale	N/A	80	46	18 Nov. 2019
P4PRO	Breeding-scale	N/A	100	35	18 Nov. 2019
P4PRO	Breeding-scale	N/A	120	30	18 Nov. 2019
P4RTK	Breeding-scale	Enabled	25	371	16 Oct. 2019
P4RTK	Breeding-scale	Enabled	40	171	16 Oct. 2019
P4RTK	Breeding-scale	Enabled	60	102	16 Oct. 2019
P4RTK	Breeding-scale	Enabled	80	76	16 Oct. 2019
P4RTK	Breeding-scale	Enabled	100	56	16 Oct. 2019
P4RTK	Breeding-scale	Enabled	120	43	18 Nov. 2019
P4RTK	Breeding-scale	Disabled	25	372	18 Nov. 2019
P4RTK	Breeding-scale	Disabled	40	171	18 Nov. 2019
P4RTK	Breeding-scale	Disabled	60	102	18 Nov. 2019
P4RTK	Breeding-scale	Disabled	80	75	18 Nov. 2019
P4RTK	Breeding-scale	Disabled	100	56	18 Nov. 2019
P4RTK	Breeding-scale	Disabled	120	43	18 Nov. 2019
PRRTK	Breeding-scale	Enabled	25	194	14 Jan. 2020
PRRTK	Breeding-scale	Enabled	40	106	14 Jan. 2020
PRRTK	Breeding-scale	Enabled	60	64	14 Jan. 2020
PRRTK	Breeding-scale	Enabled	80	48	14 Jan. 2020
PRRTK	Breeding-scale	Enabled	100	35	14 Jan. 2020
PRRTK	Breeding-scale	Enabled	120	36	14 Jan. 2020
PRRTK	Breeding-scale	Disabled	25	194	14 Jan. 2020
PRRTK	Breeding-scale	Disabled	40	106	14 Jan. 2020
PRRTK	Breeding-scale	Disabled	60	64	14 Jan. 2020
PRRTK	Breeding-scale	Disabled	80	48	14 Jan. 2020
PRRTK	Breeding-scale	Disabled	100	35	14 Jan. 2020
PRRTK	Breeding-scale	Disabled	120	36	14 Jan. 2020
P4PRO	Production-scale	N/A	80	1922	26 Oct. 2019
P4PRO	Production-scale	N/A	100	1231	26 Oct. 2019
P4PRO	Production-scale	N/A	120	888	26 Oct. 2019
P4RTK	Production-scale	Enabled	80	1882	26 Oct. 2019
P4RTK	Production-scale	Enabled	100	1252	26 Oct. 2019
P4RTK	Production-scale	Enabled	120	930	26 Oct. 2019

Note. Summary of flight information including the small unoccupied aircraft system (sUAS) that was used, the field that was flown, whether the real-time kinematic (RTK) global positioning system was enabled on the Phantom 4 RTK sUAS, the altitude (m) above ground level that each flight mission was conducted, and the number of images collected for each flight.

GCPs placed at the corners of the field (149, 153, 169, and 173); (e) four GCPs placed at the corners and one placed at the center (149, 153, 161, 169, and 173); and (f) all 25 of the GCPs (149–173) (Figure 3). In addition, the same GCP configurations were tested in the breeding-scale and production-scale fields to determine if different GCP configurations reduced the altitudinal (Z) error (Figures 2 and 3).

2.4 | Image Processing in Pix4D, Agisoft Metashape, and OpenDroneMap

For the purposes of this study, a "georeferencing scenario" or "scenario" refers to a given GCP configuration for a specific altitude conducted with one of the two sUAS over one of the field study areas. Image processing for all these
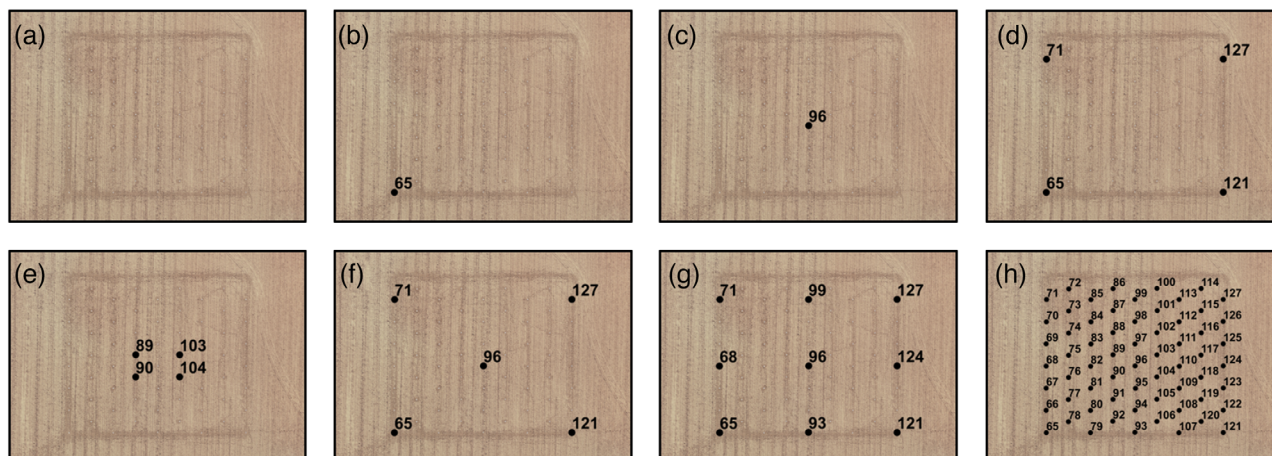
FIGURE 2 Ground control points (GCPs) configurations of the breeding-scale field. Eight different GCP configurations used when processing images of the breeding-scale field in Pix4Dmapper photogrammetry software. Ground control point configurations include no GCPs (a), 1 corner GCP (b), 1 middle GCP (c), 4 corner GCPs (d), 4 middle GCPs (e), 5 GCPs (f), 9 GCPs (g), and all 63 GCPs (h). Labels indicate which GCPs were used for each configuration. The breeding-scale field was centered on the coordinates of 408242.279, 3661040.007 (WGS84/UTM Zone 12N)
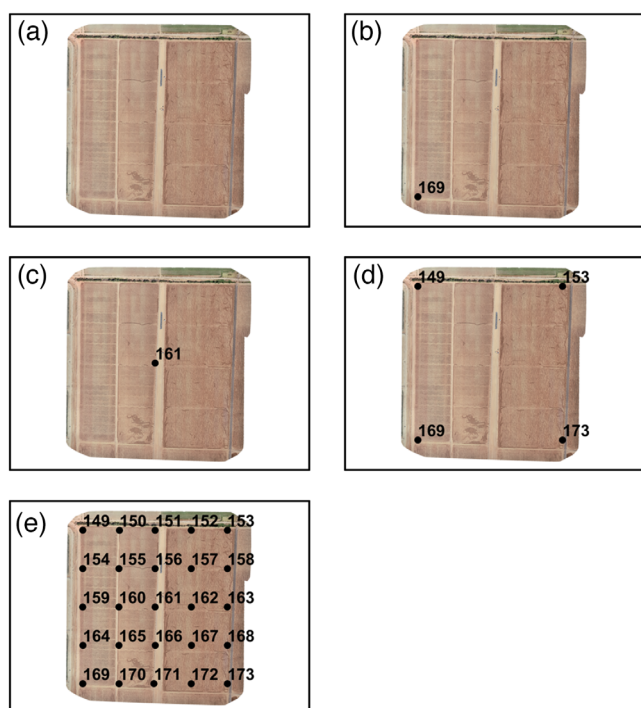

FIGURE 3 Ground control points (GCPs) configurations of the production-scale field. Five different GCPs configurations used when processing the production-scale field flights in Pix4Dmapper photogrammetry software. Ground control point configurations include no GCPs (a), one corner GCP (b), one middle GCP (c), four corner GCPs (d), and all 25 GCPs (e). Labels indicate which GCPs were used for each configuration. The production-scale field was centered on the coordinates of 408388.680, 3661075.562 (WGS84/UTM Zone 12N)

scenarios was conducted using Pix4Dmapper (Pix4D, Version 4.4.12), while a subset of 12 of the scenarios were also processed using Agisoft Metashape (Agisoft LLC, Version 1.6.1) and OpenDroneMap (ODM; Version 0.3.1) software for com-

parison purposes. OpenDroneMap is open-source software, whereas Pix4Dmapper and Agisoft Metashape are commercial software packages with licensing fees. In Pix4Dmapper, the "3D Maps" default template was used for all the processing for the P4PRO and P4RTK flights. The processing in Pix4D was done in the following order: (a) initial processing, where key points were extracted and matched and a tie point cloud was created; (b) GCP placement and camera optimization; (c) dense cloud reconstruction and creation of a 3D textured mesh; (d) creation of a digital surface model, or DSM; and (e) creation of an orthomosaic based on orthorectification. The initial processing, in which a ray cloud is constructed, was conducted using the default settings for 15 of the 36 flights that were conducted. For the 21 P4PRO flights and non-RTK flights conducted with the P4RTK, the settings were adjusted to force the optimal internal parameters to be close to original values prior to initial processing to ensure that the ray cloud was constructed properly. This was altered to ensure that initial processing finished with under 5% relative difference between initial and optimized internal camera parameters as recommended by Pix4D. For the scenarios where GCPs were used for georeferencing, GCPs were loaded, and the rematching and optimization tool was used immediately following the initial processing steps. The GCPs were identified by selecting them manually in at least two of the image tiles, and then the automatic marking feature available within Pix4Dmapper was used to select them in the rest of the image tiles. There were occasionally GCPs in the validation data that were not able to be automatically identified using Pix4Dmapper's automatic marking feature. This was because dust had collected on the surface of many of the GCPs between collection of the original and validation data sets. If the automatic marking feature failed to properly identify a GCP location in the validation data, GCPs were manually identified in all images

so that consistent use of GCPs was maintained among image sets. The next stage of processing, where the point cloud and 3D textured mesh were constructed, was performed immediately after georeferencing was completed. Finally, a DSM and an orthomosaic were generated that could be used for further analyses.

After georeferencing in Pix4Dmapper was completed, the image pixel coordinates of GCP locations in the image tiles, as during Pix4DMapper processing, were exported from the software, so identical GCP data could be used for processing with other photogrammetry software. For example, to georeference images in ODM, a text file (gcplist.txt) was required to relate the geographic coordinates of the GCPs to the image coordinates in each of the images that contained a GCP. Because these data were available from prior processing with Pix4DMapper, the information was reformatted to the specifications required for ODM. This ensured that the performance of the software was compared using identical inputs to relate geographic and image coordinates for each GCP. OpenDroneMap was run from the command line using the software's Docker image (Merkel et al., 2014). Default settings were used except for the "orthophoto-resolution" setting, which was specified to the resolution of orthomosaic output from Pix4DMapper to facilitate fair comparisons between the software. As with the commercial photogrammetry software, the general workflow in ODM progressed in five steps: (a) sparse point cloud of ties points using OpenSfM; (b) densification of the point cloud; (c) meshing to create a 3D surface; (d) texturing using image overlay; and (e) orthophoto construction.

Processing in Agisoft Metashape was done by following a similar workflow that was used for Pix4Dmapper. Settings were chosen to match the default settings used for 3D Maps in Pix4Dmapper, and similar steps were taken to generate the resulting orthomosaics. The general workflow in Metashape progressed in five general steps: (a) tie point cloud construction, (b) GCP placement and camera optimization, (c) dense cloud construction, (d) digital elevation map (DEM) construction, and (e) generation of the orthomosaic. The tie point cloud, also referred to as the sparse point cloud, was constructed by aligning the photos with the key point, and tie point limits increased from the default levels of 40,000 and 4,000 to 200,000 and 20,000, respectively. Once GCPs were placed in each scenario, they were identified in at least two images to ensure the software could automatically identify their position in all other images in which they occurred. Once all GCPs were placed into the scenario, cameras were optimized based upon the GCP locations to correct for spatial error in a similar fashion to the rematching and optimization process in Pix4Dmapper. To accomplish this, all the cameras were deselected and GCPs were selected before optimization was used. To attempt to match the default settings for the generation of 3D maps in Pix4Dmapper, the dense cloud

was processed at medium quality with aggressive depth filtering. Once the dense point cloud was constructed, a DEM was constructed using the dense point cloud with interpolation enabled. The orthomosaic was based on the DEM and was processed using the mosaic blending mode with hole filling enabled. The DEM and final orthomosaic were both constructed using the same UTM projection as the rest of the georeferencing scenarios in this study (WGS84/UTM Zone 12N). The processing in Pix4Dmapper, ODM, and Agisoft Metashape was performed using a computer with an Intel Xeon® CPU E5-2630 v3 (two processors) and 256 GB of installed RAM.

2.5 | Extraction of X, Y, and Z location data using QGIS software

To extract location data from each orthomosaic and DSM for the image sets defined in Table 1, the orthomosaics generated in Pix4Dmapper, Metashape, and ODM were loaded into QGIS software v.3.8.3 (https://www.qgis.org/). To estimate two-dimensional (2D), horizontal accuracy (i.e., X/Y positional error), the GCP locations in each orthophoto were identified, manually marked, and added as a point feature in a new point layer shapefile. To ensure that point features were placed consistently, the project zoom was increased until a point that best approximated the location of the center pixel of each GCP could be selected. The UTM coordinates of each manually-selected point were then exported from the attribute table of the shapefile layer. These UTM coordinates were compared with the known coordinates measured for each of the GCPs in the field, as described in the Data Analysis and Statistics section.

Altitudinal data (Z) were obtained for each GCP using the DSM generated for each project in Pix4Dmapper. The locations of the GCPs identified in each of the orthomosaics were used as the point for which altitude estimates were extracted. Then, the DSM was placed in the QGIS project, and the altitude estimates were extracted from the DSM using the Point Sampling Tool plugin. As with the X/Y locations, these estimates of altitude based on the DSM were then compared to the altitude values that were recorded using the Trimble RTK-GPS at GCP locations prior to the flight missions.

2.6 | Data analysis and statistics

The GCP coordinates from each orthomosaic were exported from QGIS, and they were associated with the measured GCP coordinates as recorded by the RTK-GPS prior to the flight missions. An estimate of two-dimensional horizontal error was calculated using the following equation (i.e., the distance formula): $d = \sqrt{([x_2 - x_1]^2 + [y_2 - y_1]^2)}$, where d is

the estimated two-dimensional error (in meters), x_1 is the X coordinate of the point exported from QGIS, x_2 is the measured X coordinate at the physical center of the GCP in the field, y_1 is the Y coordinate of the point exported from QGIS, and y_2 is the measured Y coordinate the physical center of the GCP in the field. To estimate Z error, the absolute value of the difference between the field-measured altitude and the altitude estimated from the DSM was used.

The means of the error estimates were graphed using the ggplot2 package in R software (R Development Core Team, 2011; Wickham, 2016). In addition, postplots that showed the spatial error among GCPs were produced in QGIS for the breeding-scale field using the flights conducted with the P4PRO and P4RTK at 60 m altitude AGL and for each GCP configuration. The same process was used to produce postplots for altitudinal error in the production-scale field for the flights conducted with the P4PRO and P4RTK at 100 m altitude AGL and for each GCP configuration. To better visualize differences between these configurations in the breeding-scale and production-scale postplots, the diameter of the postplot icons was specified as the computed error +1 m and error +10 m, respectively.

To assess the consistency of X/Y spatial error estimates for flights conducted in the fall of 2019 (the original data set) versus those flights conducted in the early spring of 2020 (the validation data sets) over the breeding-scale field, two-sided, paired *t*-tests were carried out using the "t.test" function in R with a 95% confidence interval (R Development Core Team, 2011). To carry out the tests, the error estimates for each individual GCP from the six flight altitudes, GCP configurations, and RTK settings were treated as paired data with pairs being "original" and "validation" GCP error estimates.

Comparisons of software processing time and performance were carried out using the same above-mentioned workstation for processing. A subset of georeferencing scenarios was selected amongst the two drone platforms, with RTK enabled and disabled, at two flight altitudes (25 and 120 m), and with four or zero GCPs used for georeferencing. After completion of the processing for each scenario using each of the respective software, the total processing time was recorded and the georeferencing errors associated with individual GCPs were compared. Nonparametric Kruskal-Wallis tests were performed in Python v3.9 using the command "scipy.kruskal" from the SciPy library to determine if there were significant differences in the mean georeferencing errors among the three software (Virtanen et al., 2020). To further assess differences, nonparametric, pairwise comparisons of georeferencing errors were performed using Conover tests (if the Kruskal-Wallis null hypothesis was rejected) using the "scikit_poshocs.posthoc_conover" from the Scikit library (Terpilowski, 2019).

3 | RESULTS

3.1 | Two-dimensional georeferencing accuracy

The flights conducted at all six altitudes over the breeding-scale field using the P4PRO exhibited a similar pattern of decreasing spatial error as the number of GCPs used for georeferencing increased from 0 to 63 (Figure 4a). Regardless of flight altitude, it was clear that forgoing the use of GCPs led to poor performance with spatial error estimates ranging from a minimum of 1.48 m for the 40 m altitude up to 2.28 m for the 25 m altitude (Figure 4a). The use of one GCP, either in the corner or center of the field, resulted in across-altitude mean error estimates of 0.80 to 0.35 m, respectively. The four corner, five, and nine GCP configurations all had across-altitude mean error estimates of 0.03 m while using all 63 GCPs produced the same spatial mean error estimate of 0.03 m (Figure 4). The configuration of four middle-of-the-field GCPs resulted in a slight increase in georeferencing error with a mean error estimate of 0.04 m. These results demonstrate that, on average, increasing the number of GCPs used for georeferencing to more than four per 0.4-ha study area did not provide any gain in geospatial accuracy.

For flights conducted using the P4RTK with RTK enabled, a similar trend was observed as with the P4PRO. Configurations using four or more GCPs resulted in an across-altitude mean error estimate of 0.03 m while configurations using only one GCP, either in the corner or the center, resulted in spatial error accuracies of 0.06 m and 0.05 m, respectively (Figure 4b). However, the largest difference for geospatial accuracy when compared with the flights conducted with P4PRO was observed for the zero GCP configuration; with RTK enabled, the mean error estimate across altitudes was 0.07 m whereas for the P4PRO it was 1.77 m, a 25-fold difference in accuracy. Furthermore, the error estimates for the P4RTK with RTK enabled varied between 0.03–0.08 m (SD = 0.02 m) among the GCP configurations (including zero GCPs) compared with a range of 0.02–2.28 m (SD = 0.61 m) using the P4PRO (Figure 4a, 4b). Not only was the range and standard deviation of the error estimates for the P4RTK with RTK enabled much smaller than that observed for the P4PRO, but the addition of GCPs had less impact on reducing the georeferencing error as well. The difference in across-altitude mean error for zero GCPs and four corner GCPs was 0.04 m for the P4RTK whereas for the P4PRO, that difference was 1.74 m. Thus, the use of GCPs results in an improvement in georeferencing accuracy but it is less pronounced when using the Phantom 4 RTK with RTK enabled.

For the P4RTK flights with RTK disabled, the use of four or more GCPs was effective at improving georeferencing accuracy. The across-altitude error estimates were identical to that
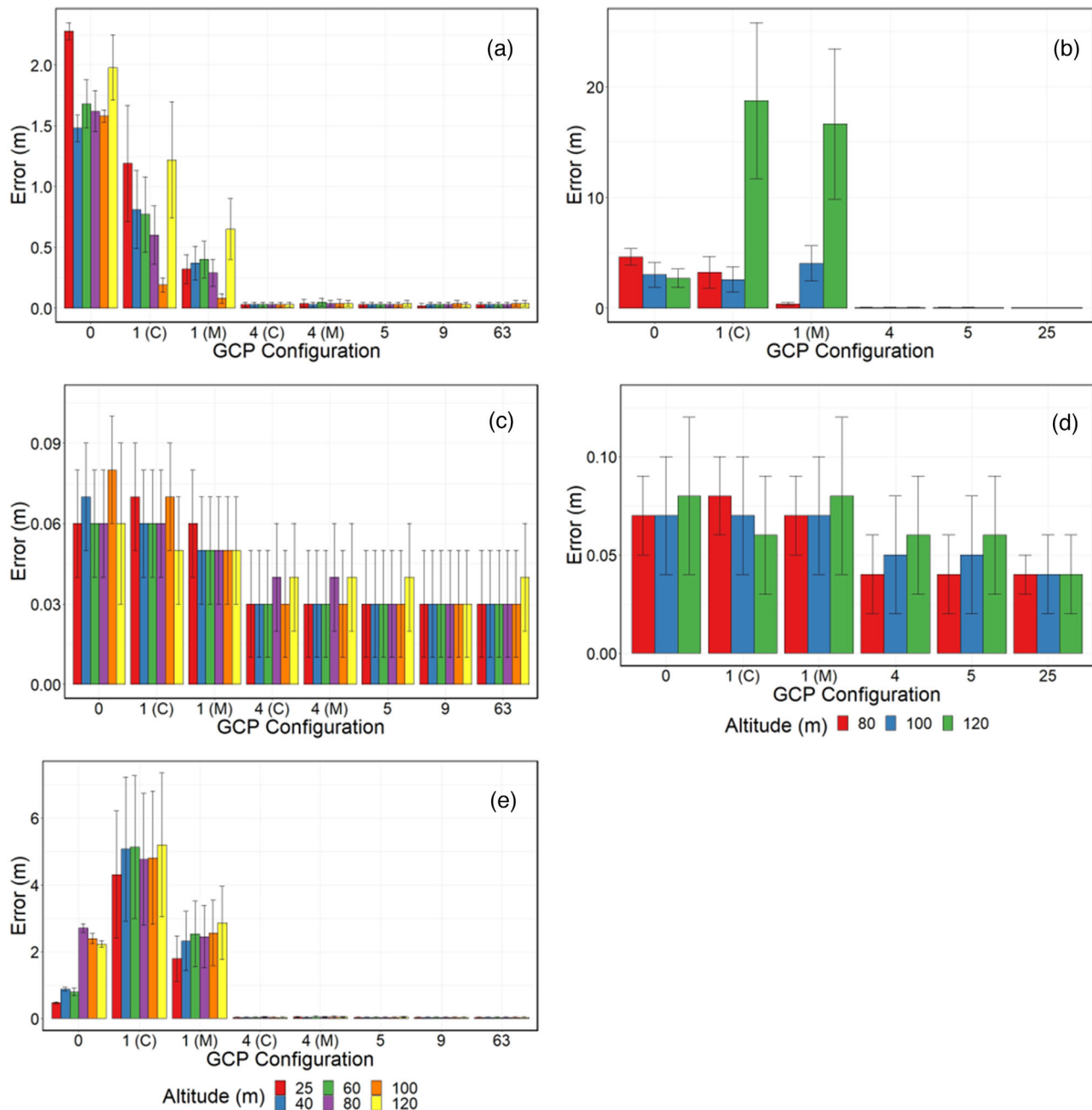
FIGURE 4   Mean geospatial accuracy. The mean error (m) and standard deviation (m) of the flights conducted for the breeding-scale field with the Phantom 4 Pro (a), the breeding-scale field with the Phantom 4 real-time kinematic (RTK) with RTK enabled (b), the breeding-scale field with the Phantom 4 RTK with RTK disabled (c), the production-scale field with the Phantom 4 Pro (d), and the production-scale field with the Phantom 4 RTK with RTK enabled (e). Accuracy was calculated using the Universal Transverse Mercator (UTM) coordinates of each ground control point (GCP) postprocessing and the coordinates collected for each GCP on the ground using a Trimble RTK global positioning system (RTK-GPS). The flights were conducted at altitudes of 25, 40, 60, 80, 100, and 120 m AGL for the breeding-scale field and at 80, 100, and 120 m AGL for the production-scale field. Eight GCP configurations are shown: no GCPs (0), 1 corner GCP (1 C), 1 middle GCP (1 M), 4 corner GCPs (4 C), 4 middle GCPs (4 M), 5 GCPs, 9 GCPs, and all 63 or 25 GCPs for the breeding-scale and production-scale fields, respectively (63 and 25)

of the P4PRO for four of the GCP configurations; the four corner, five, and nine GCP configurations resulted in an across-altitude error estimates of 0.03 m, whereas the configuration with four middle-of-the-field GCPs had an error estimate of 0.04 m (Figure 4c). However, in stark contrast to the

P4PRO and P4RTK with RTK enabled, the accuracy of the P4RTK with RTK disabled displayed greater errors for the zero, one corner, and one center GCP configurations; the error estimates were 1.58, 4.88, and 2.42 m, respectively. As discussed below, this result is likely related to issues of image

translation without rescaling that occurs when only one GCP is used for georeferencing.

Georeferencing accuracy of P4PRO images over the production-scale field followed similar trends to those observed with the breeding-scale field; the use of four corner GCPs achieved nearly the same georeferencing error as using all 25 GCPs, 0.06 m and 0.04 m, respectively (Figure 4d). In addition, this level of georeferencing accuracy, 0.04 m, for the production-scale field using four GCPs was comparable with that of the breeding-scale field, which had an across altitude mean error estimate of 0.03 m. Although the error estimates for four GCPs in the production-scale field was nearly double that of the breeding-scale, 0.06 m vs. 0.03 m, the study area of the production field was more than 160 times larger, highlighting the efficacy of GCPs for georeferencing at multiple scales. Interestingly, the largest georeferencing errors were not found when GCPs were excluded from the processing but instead were found when using only one GCP, either in the corner or in the middle of field, for georeferencing the 120 m altitude flights (Figure 4d). These two configurations produced across-altitude error estimates of 18.75 m for the one corner GCP and 16.64 m for the middle-of-the-field GCP layouts, which were the highest observed spatial 2D error estimates in the study. The increase in georeferencing error when using only one GCP, either in the corner or middle of the field, is likely related to the issue of image translation without necessary rescaling, which is discussed below.

Georeferencing accuracy of the P4RTK images over the production-scale field was improved compared with the P4PRO—all configurations had across-altitude error estimates less than 1 m with the highest observed error being 0.08 m (Figure 4e). In addition, the inclusion of four corner GCPs, the configuration with the lowest georeferencing error, reduced the spatial error from 0.08 m for zero GCPs to 0.05 m (across altitude mean), a difference of only 3 cm. The difference in georeferencing accuracy of the P4RTK relative to the P4PRO was also quite significant for the production-scale field; the P4PRO had error estimates ranging from 0.04 to 18.75 m (SD = 5.55 m), whereas the P4RTK had values ranging from 0.04 to 0.08 m (SD = 0.02 m). The use of all 25 GCPs had the lowest georeferencing error estimates with values of 0.04 m found for all three flight altitudes. As was obtained for the P4RTK over the breeding-scale field, the difference in error between using no GCPs and using four was small; a mean difference of 0.04 m was observed across the three altitudes flown.

3.2 | Altitudinal georeferencing accuracy

In assessing the accuracy of the altitude positional coordinates (Z-axis), the results were similar as that for the X/Y geospatial coordinates, where four GCPs provided a substantial reduction in mean errors (Figure 5). However, only minimal improvements were observed with the addition of GCPs past four in each scenario (Figure 5). For the flights conducted over the breeding-scale field with the P4PRO, the across-altitude, mean Z-axis error was 2.79 m with error estimates ranging from 0.32 to 6.85 m when no GCPs were used in processing. When the four corner GCPs were used for georeferencing, the mean Z-axis error was only 0.03 m (values ranging from 0.01 to 0.07 m) representing a 93-fold reduction in altitudinal error estimates (Figure 5a). When all 63 GCPs were used for processing, the across-altitude mean Z-axis error was 0.01 m.

For scenarios using the flight imagery collected with the P4RTK, the across-altitude, mean Z-axis error for the no-GCP configuration was 1.97 m. Although this is only a difference of 0.82 m relative to the P4PRO, there was considerably less variability in accuracies across the different altitudes – the range of accuracies for the P4PRO was 6.53 m compared to 0.16 m for the P4RTK (Figure 5b). Additionally, the incorporation of one GCP, either in the corner or the middle of the field, reduced the mean Z-axis errors across all altitudes to levels comparable to the four, five, and all-GCPs configurations (0.04 m compared to 0.03, 0.02, and 0.02 m, respectively). When all 63 GCPs were included for processing, the across-altitude mean Z-axis error was 0.02 m, a one-centimeter increase with respect to the P4PRO flights.

Flights conducted with the P4PRO over the production-scale field exhibited variability with respect to Z-axis error estimates; however, the general trend held that use of four corner GCPs provided appreciable reductions in error estimates (Figure 5c). When four or more GCPs were not used for georeferencing, there was a clear impact of the flight altitude on the Z-axis errors. Across the none, one-corner, and one middle-of-the-field GCP configurations, the mean errors associated with the 120, 100, and 80 m flights were 69.30, 13.12, and 3.59 m, respectively. Including 4, 5, and all 25 GCPs resulted in across-configuration Z-axis errors for the 120, 100, and 80 m flights of 0.68, 0.71 and 0.04 m, respectively, demonstrating the effect of GCPs on improving georeferencing.

Like the results obtained on the breeding-scale field with the P4RTK, the across-altitude mean Z-axis error of the no-GCP configuration for the production scale field was 1.86 m, 11 cm less than that for the breeding-scale field. Also consistent with the breeding-scale results, there was limited variation for Z-axis errors within the three altitudes at which flights were conducted (Figure 5d). The use of four corner GCPs resulted in an across-altitude mean Z-axis error of 0.05 m while using all 25 GCPs decreased that error to a mean value of 0.04 m across the three altitudes. Finally, when comparing the altitudinal accuracy of the 25 GCPs configurations between the P4PRO and the P4RTK flights of the production-scale field, there was only a 0.01-m difference
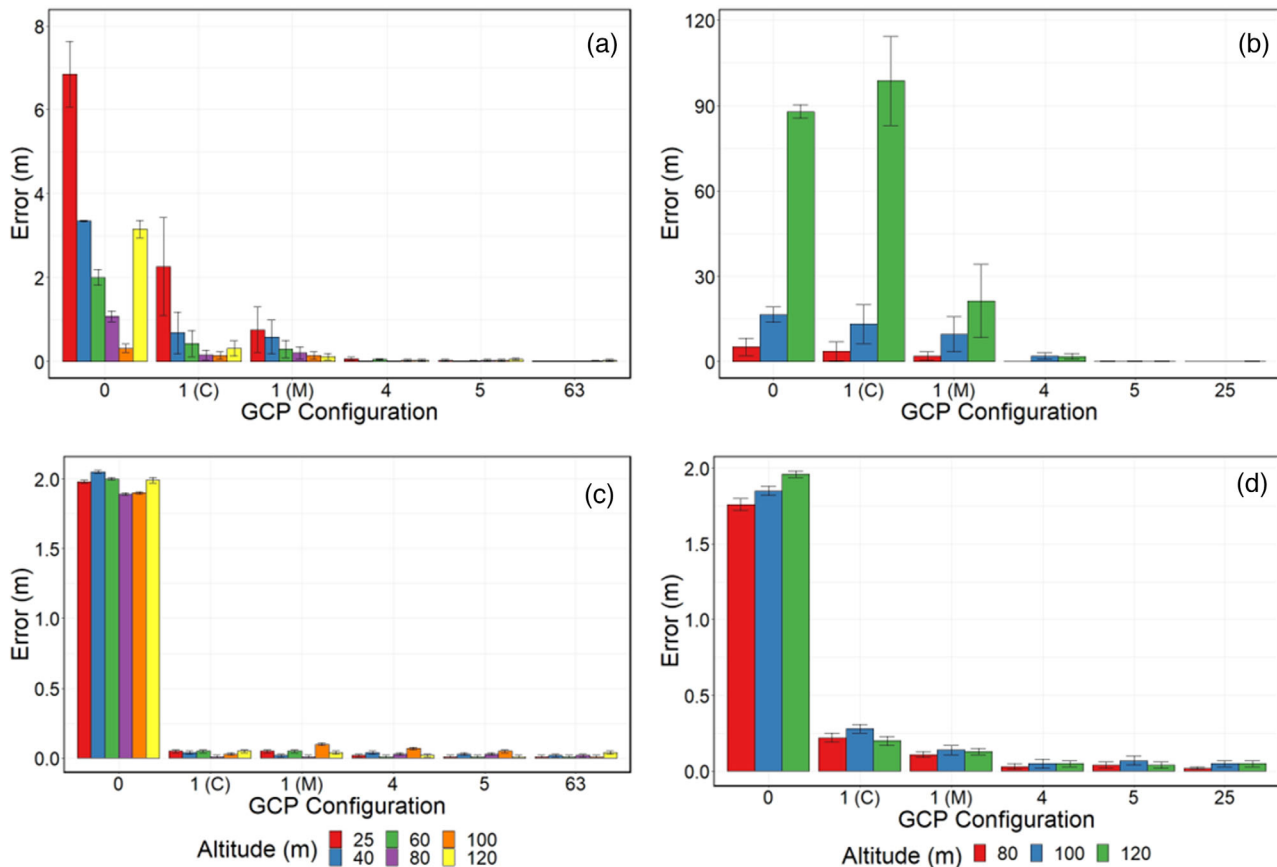
FIGURE 5 Mean altitudinal accuracy. The mean error (m) and standard deviation (m) for altitude (m) above ground level (AGL) for the flights over the breeding-scale field using a Phantom 4 Pro (a) over the breeding-scale field with the Phantom 4 real-time kinematic (RTK) with RTK enabled (b), over the production-scale field with the Phantom 4 Pro (c), and over the production-scale field with the Phantom 4 RTK with RTK enabled (d). The flights were conducted at altitudes of 25, 40, 60, 80, 100, and 120 m AGL for the breeding-scale field and at 80, 100, and 120 m AGL for the production-scale field. Six ground control point (GCP) configurations are shown: no GCPs (0), one corner GCP (1 C), one middle GCP (1 M), four corner GCPs (4), five GCPs (5), and all 63 or 25 GCPs for the breeding-scale and production-scale fields, respectively (63 and 25)

(mean accuracy of 0.05 m for the P4PRO and 0.04 m for the P4RTK).

3.3 | Effects of GCP configurations on geospatial accuracy

The 2D geospatial variability associated with individual GCPs in the breeding-scale field displayed notable differences among the different GCP configurations when images were captured by the P4PRO at 60-m altitude (Figure 6). In addition, the variability associated with individual GCPs exhibited spatial trends based on the configuration used. When using no GCPs, the error around each GCP was comparatively high across the field (mean error of 1.68 m); however, this error was not consistent. There was an increase in mean spatial error across the columns of GCPs ranging from 1.42 m on the west side of the field to 1.99 m on the east. Traveling north to south, the row error means decreased from 1.79 to 1.60 m (Figure 6a).

For the configurations where only one GCP was used, either in the center or southwest corner of the field, there were linear trends in the geospatial error associated with individual GCPs relative to the GCP used for georeferencing. For the one corner GCP configuration (using GCP 65), the error ranged from a minimum of 0.02 m for GCP 65 to a maximum of 1.29 and 1.35 m for GCPs 114 and 127, respectively. The geospatial error associated with the GCPs increased in an approximately monotonic fashion moving diagonally across the field from the southwest corner to the northeast at a value of 0.13 m (Figure 6b). For the middle-of-the-field configuration, GCP 96 (used for georeferencing) had a spatial error of 0.14 m, and the mean error values increased by approximately 0.12 m moving in a concentric circle pattern away from the center GCP reaching a maximum spatial error of 0.63 m (mean of corner GCPs) at the corners of the field (Figure 6c).

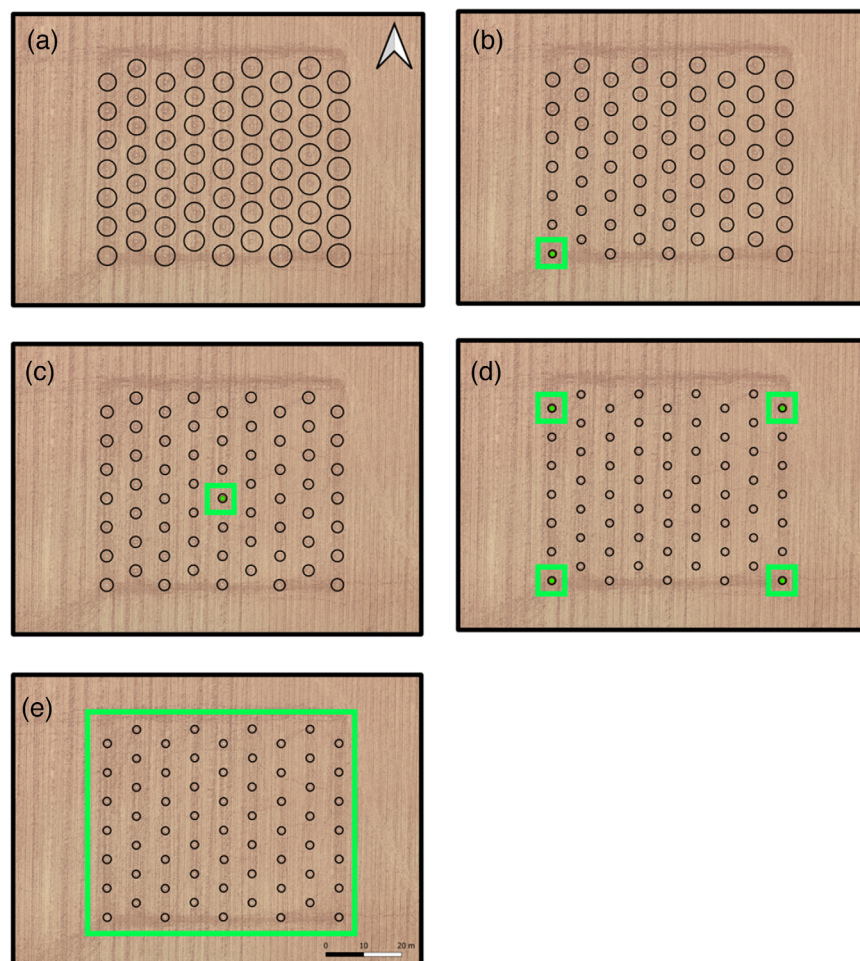The use of four corner GCPs and all 63 GCPs performed comparably; the mean error across all individual GCPs for

FIGURE 6 Geospatial accuracy of individual ground control points (GCPs) Using the Phantom 4 PRO. Spatial distribution of georeferencing accuracy among GCPs in five different GCPs configurations for flights performed over the breeding-scale field at 60 m above ground level. The radii of the circles represent the error of each GCP increased by adding a constant of 1 m for visual enhancement. Five GCP configurations are shown: no GCPs (a); one corner GCP, 65(b); one middle GCP, 96 (c); four corner GCPs, 5, 71, 121, 127 (d); and all 63 GCPs (e). Green indicates selected GCPs for georeferencing, except for E where all 63 were used

both configurations was 0.03 m and both configurations had a standard deviation of 0.02 m (Figure 6d, 6e). The mean error for both rows and columns ranged from 0.02 to 0.04 m and 0.01 to 0.04 m, respectively, with no apparent spatial trend in how errors were distributed, suggesting that the spatial error was consistent throughout the field area in both configurations. The geospatial variability associated with individual GCPs from the P4RTK flights of the breeding-scale flight at 60-m altitude did not exhibit significant differences amongst the configurations tested nor were any spatial trends apparent in the errors associated with GCPs across the field area (Supplemental Figure S1). When no GCPs were used, the mean spatial error associated with both the rows and columns of GCPs was 0.06 m with minimal variation among them (SD = 0.01 m; Supplemental Figure S1A). The one-corner and middle-of-the-field GCP configurations performed similarly; the mean error for both rows and columns of GCPs were 0.06 and 0.05 m, respectively, with no trend among the individual rows/columns. The configurations utilizing the four corner GCPs and all 63 of the GCPs produced similar results, where mean spatial error across both rows and columns of GCPs was 0.03 m with no observable trends across the field in either direction highlighting the spatial consistency of the georeferencing capabilities of the P4RTK.

The spatial altitudinal accuracy in the production-scale field was also investigated because there was greater variation in altitude estimates within that field compared with the breeding-scale field. To determine spatial differences in accuracy, the effects of GCP configuration on Z-axis accuracy were investigated. The variability in altitudinal georeferencing accuracy for scenarios using images captured by the P4PRO exhibited similar spatial trends in error as for the X/Y variability in the breeding-scale field despite the difference in the plane of measurement and study area size. When using no GCPs, the mean Z-axis error for the 100-m flight was 16.85 m, however, the error increased across columns of GCPs from the west side to the east side of the field by a mean value of 7.52 m (12.89 m for the western column of GCPs to 20.41 m for the east, Figure 7); there was negligible change from the north to the south edge of the study area. When using the single corner GCP (169), the error increased diagonally across the GCPs, at a mean value of 0.94 m, to the northeast corner where it reached a maximum value of 27.64 m (Figure 7b). Using just the middle-of-the-field GCP (161), the Z-axis error increased in all directions moving away from the center GCP and reached maximum values of 21.29, 22.39, 16.32, and 10.39 m for the northwest, northeast, southwest, and southeast corners, respectively (Figure 7c). Using four corner GCPs
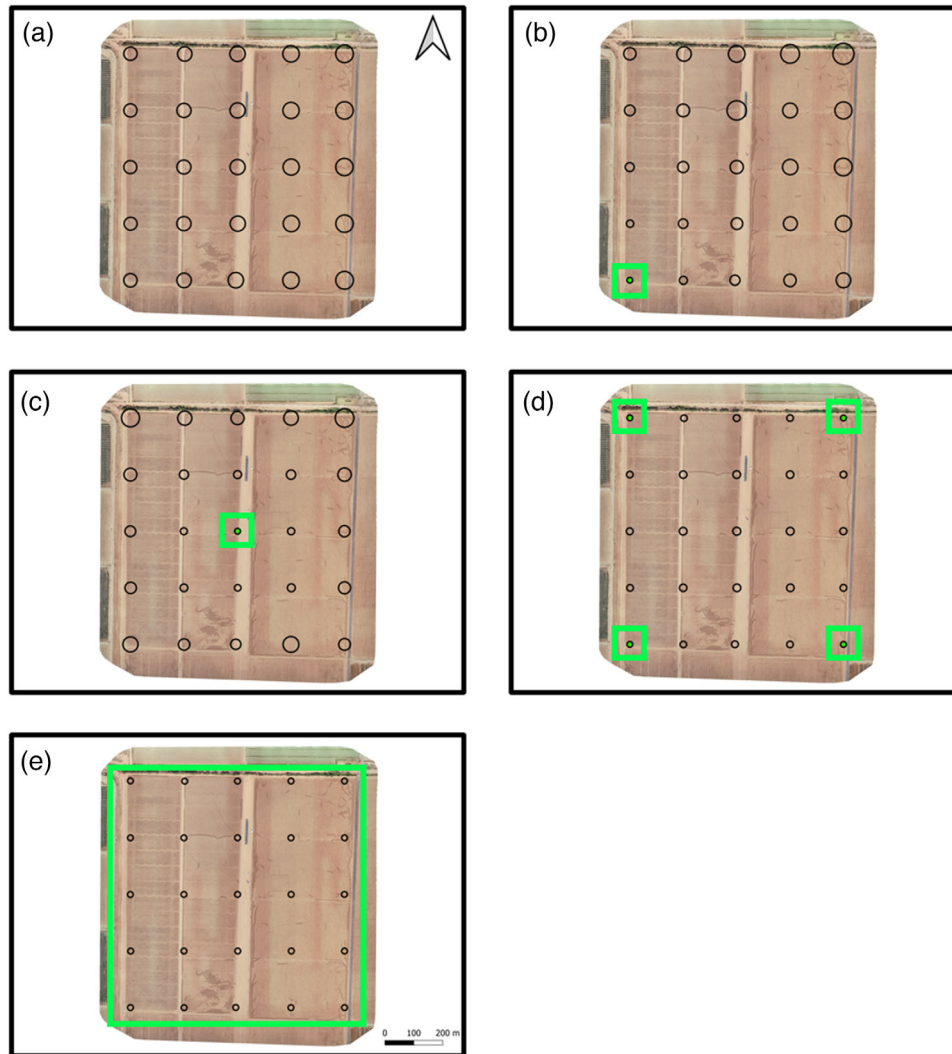
FIGURE 7 Altitudinal accuracy for individual ground control points (GCPs) using the Phantom 4 Pro. Spatial distribution of georeferencing accuracy for altitude among GCPs in five different GCPs configurations for flights performed over the production-scale field at 100 m above ground level using the Phantom 4 Pro small unoccupied aircraft system (sUAS). The radii of the circles represent the altitudinal error of each GCP increased by adding a constant of 10 m for visual enhancement. Five GCP configurations are shown: no GCPs (a); one corner GCP, 169 (b); one middle GCP, 161 (c); four corner GCPs, 149, 153, 169, 173 (d); and all 25 GCPs (e). Green indicates selected GCPs for georeferencing, except for E where all 25 were used

resulted in a mean Z-axis error of 1.98 m across the field, but with respect to rows and columns, there were spatial trends. Moving south to north (row 1 to row 5, respectively) across rows of GCPs, mean Z-axis errors increased from 0.94 m for row 1 to 3.03 m for row 3, and then finally back to 0.95 m for row 5. This same trend was observed across columns of GCPs as well; column 1 on the west side of the field had a mean error of 1.01 m increasing to 2.87 m for column 3, and finally 1.17 m for column 5 on the east side of the field (Figure 7d). Finally, when all GCPs were used for processing, the Z-axis mean error was 0.05 m, which was consistent across the field without any trends or patterns observed (Figure 7e).

For the Z-axis error estimates from the imagery collected with the P4RTK with RTK enabled, there were no observed spatial trends in the altitudinal errors associated with the individual GCPs for any of the GCP configurations (Supplemental Figure S2). In fact, with respect to row and column error means within each configuration, the obtained mean altitudinal error values were nearly identical. The only observed differences for mean error accuracy were those associated with different GCP configurations discussed above.

3.4 | Validation of breeding-scale field accuracy estimates

To assess the consistency of error estimates, a second set of flights was conducted on the breeding-scale field in January of 2020 using the P4RTK with RTK both disabled and enabled

TABLE 2   Comparison of original and validation data

RTK	Altitude	GCPs	Original		Validation			
			Mean	SD	Mean	SD	*t*-value	MED
				m				m
Enabled	25	None	0.06	0.02	0.04	0.02	7.38***	0.02
Enabled	25	Four	0.03	0.02	0.03	0.02	3.27**	0.00
Enabled	40	None	0.07	0.02	0.04	0.02	8.99***	0.02
Enabled	40	Four	0.03	0.02	0.03	0.02	1.02	0.00
Enabled	60	None	0.06	0.02	0.04	0.02	5.25***	0.01
Enabled	60	Four	0.03	0.02	0.03	0.02	1.16	0.00
Enabled	80	None	0.06	0.02	0.04	0.02	6.31***	0.02
Enabled	80	Four	0.04	0.02	0.03	0.02	3.09**	0.01
Enabled	100	None	0.08	0.02	0.04	0.02	12.03***	0.04
Enabled	100	Four	0.03	0.02	0.04	0.02	6.30***	0.01
Enabled	120	None	0.06	0.03	0.04	0.02	6.38***	0.02
Enabled	120	Four	0.04	0.02	0.04	0.02	0.35	0.00
Disabled	25	None	0.48	0.03	1.15	0.08	90.98***	0.66
Disabled	25	Four	0.03	0.02	0.03	0.02	1.69	0.00
Disabled	40	None	0.88	0.05	0.73	0.07	13.13***	0.15
Disabled	40	Four	0.03	0.02	0.03	0.02	0.17	0.00
Disabled	60	None	0.80	0.11	3.60	0.13	224.18***	2.79
Disabled	60	Four	0.03	0.02	0.03	0.02	1.59	0.00
Disabled	80	None	2.71	0.13	0.54	0.06	186.10***	2.18
Disabled	80	Four	0.04	0.02	0.03	0.02	1.09	0.00
Disabled	100	None	2.39	0.15	1.34	0.20	25.50***	1.06
Disabled	100	Four	0.03	0.02	0.03	0.02	2.91**	0.01
Disabled	120	None	2.23	0.10	0.79	0.16	45.17***	1.43
Disabled	120	Four	0.03	0.02	0.04	0.02	3.07**	0.01

Note. Mean georeferencing error and SD for the accuracy of the ground control point (GCP) locations in the breeding-scale field for the original data taken in 2019 as well as the validation data taken in 2020 when compared with known Universal Transverse Mercator (UTM) coordinates collected on the ground. Information is given on whether the real-time kinematic global positioning system (RTK-GPS) was enabled or disabled, the flight altitude (m) above ground level of the flight, the GCP configuration that was used, the *t*-value based upon a paired sample *t*-test and its significance level, and the mean error difference (MED, m) between the original and validation data (MED, m).

*Significant at the < .05 level. **Significant at the < .01 level. ***Significant at the < .001 level.

at all six altitudes. For the comparison, the zero and four corner GCP configurations were used. The results indicated that across the two timepoints, Fall 2019 ("Original") and Winter 2020 ("Validation"), there were significant ($P < .05$) differences in the mean error estimates with respect to both the RTK and GCP configurations (Table 2). With RTK enabled, 9 out of the 12 scenarios exhibited significant differences in mean error estimates; whereas with RTK disabled, 8 of the 12 georeferencing scenarios exhibited significant differences. The mean error difference between the two timepoints when comparing RTK enabled versus disabled across altitudes and GCP configurations were large; with the RTK enabled, the average difference between timepoints was 0.01 m while for the RTK disabled data, it was 0.69 m. When comparing the use of four corner GCPs versus no GCPs across timepoints, the four corner GCP configurations gave mean error differences ranging

from 0.00 to 0.01, regardless of whether RTK was enabled or disabled. In contrast, when zero GCPs were used for georeferencing, the mean error difference across timepoints was greater, ranging from 0.02 to 2.79 m; however, with RTK enabled, the range mean error differences were much less ranging from 0.01 to 0.04 m. This finding further demonstrates the high accuracy and utility of the RTK-equipped UAV.

3.5 | Comparison of photogrammetry software

Three commonly used photogrammetry software, Pix4D, Agisoft Metashape, and ODM, were compared for georeferencing accuracy. Each software was also benchmarked to compare processing times. A subset of georeferencing

T A B L E 3 Comparison of photogrammetry software

Scenario				Software							Conover test		
				Pix4D (A)		ODM (B)		Metashape (C)					
sUAS	RTK	Alt.	GCPs	Mean	SD	Mean	SD	Mean	SD	χ^2	A & B	A & C	B & C
						m							
P4PRO	–	25	None	2.28	0.07	2.28	0.06	2.28	0.06	0.16	NS	NS	NS
P4PRO	–	25	Four	0.03	0.02	0.03	0.02	0.03	0.02	0.81	NS	NS	NS
P4PRO	–	120	None	1.98	0.27	1.77	0.08	1.94	0.22	27.72***	<0.001	NS	<0.001
P4PRO	–	120	Four	0.03	0.02	0.05	0.02	0.03	0.02	39.69***	<0.001	NS	<0.001
P4RTK	Yes	25	None	0.06	0.02	0.06	0.02	0.08	0.02	27.92***	NS	<0.001	<0.001
P4RTK	Yes	25	Four	0.03	0.02	0.03	0.02	0.03	0.02	0.99	NS	NS	NS
P4RTK	Yes	120	None	0.06	0.03	0.06	0.03	0.10	0.04	36.06***	NS	<0.001	<0.001
P4RTK	Yes	120	Four	0.04	0.02	0.04	0.02	0.03	0.02	6.98*	NS	NS	<0.05
P4RTK	No	25	None	0.48	0.03	0.49	0.19	0.48	0.03	2.77	NS	NS	NS
P4RTK	No	25	Four	0.03	0.02	0.03	0.02	0.03	0.02	0.71	NS	NS	NS
P4RTK	No	120	None	2.23	0.10	3.16	0.62	2.23	0.10	91.84***	<0.001	NS	<0.001
P4RTK	No	120	Four	0.03	0.02	0.04	0.02	0.03	0.02	15.75***	<0.01	NS	<0.001

Note. Mean georeferencing error and SD for the accuracy of the ground control point (GCP) locations for georeferencing scenarios processed in Pix4D, OpenDroneMap (ODM), and Agisoft Metashape software when compared with known Universal Transverse Mercator (UTM) coordinates. Information is given on the small unoccupied aircraft system (sUAS) used, whether the real-time kinematic (RTK) global positioning system was enabled or disabled, the altitude (Alt.; m) above ground level of the flight, the GCP configuration that was used, the chi-squared value and significance based on a Kruskal-Wallis test, and the significance or nonsignificance (NS) of pairwise comparisons based on a post-hoc Conover test.

scenarios that represented a combination of sUAS platform, RTK capabilities, flight altitude, and GCP configurations were processed using the three software with comparable settings on a Windows-based workstation. The performance of the commercial software, Pix4D and Metashape, was similar with significant differences ($P < .001$) found in only two of the 12 scenarios analyzed (Table 3). In these two instances, which occurred for the P4RTK with RTK enabled with no GCPs used at an altitude of 25 and 120 m, Pix4D had lower mean georeferencing errors than Metashape. OpenDroneMap produced significantly different georeferencing error results from both Pix4D and Metashape at the 120 m height for the P4PRO and P4RTK with RTK disabled for both GCP configurations tested, suggesting that altitude has an impact on ODM's georeferencing performance. For the scenarios with RTK enabled, Pix4D and ODM produced the same mean error estimates and standard deviations while ODM and Metashape had significantly ($P < .05$) different results for three of the four scenarios evaluated. Overall, the differences among the processing software were small, often just centimeters, highlighting the similarity of the three software.

The software benchmarking associated with the above subset of scenarios were also examined. Overall, Metashape was much faster than the other two software, often by a factor of three, while Pix4D was generally faster than ODM (Table 4). The processing times scaled with the number of images in each scenario, as expected. The inclusion of four GCPs also tended to increase processing time, but for Metashape this was

typically limited to approximately 1 min; whereas for Pix4D and ODM, the increase in time was often greater, ranging from several minutes to hours.

4 | DISCUSSION

The use of UAVs in plant science and agricultural research is becoming more prevalent as the technology matures. However, despite the increased adoption of UAVs, there is limited information on best practices for the georeferencing of photogrammetry projects. Because agricultural fields often do not present the same constraints on GCP placement as in other applications, such as urban mapping, optimization of GCPs can be undertaken. In the present work, we sought to investigate how flight altitude, GCP number and placement, and processing software impact georeferencing accuracy as these are the data collection parameters that most users will have to alter to achieve experimental objectives. Other factors such as image overlap, image quality (number of pixels, number of channels, sensor size etc.), and crop under study will impact georeferencing accuracy as well but generally are not the predominant aspects influencing downstream data products. In addition, the present study was carried out using a bare field to minimize the influence of crop-specific features that could otherwise alter the stitching or image processing and to further broaden the inferential scope of the results obtained.

The number and configuration of GCPs had a measurable impact on georeferencing error, with four GCPs providing

T A B L E 4 Software benchmarking for three photogrammetry programs

sUAS	RTK	Altitude	No. of images	GCP configuration	Pix4Dmapper	OpenDroneMap	Metashape
P4PRO	N/A	25	374	None	2:50	13:57	1:31
P4PRO	N/A	25		Four	3:37	16:00	1:30
P4PRO	N/A	120	30	None	0:15	00:21	0:05
P4PRO	N/A	120		Four	0:22	00:26	0:06
P4RTK	Enabled	25	371	None	2:59	09:15	1:47
P4RTK	Enabled	25		Four	4:50	10:33	1:48
P4RTK	Enabled	120	43	None	0:20	00:26	0:06
P4RTK	Enabled	120		Four	0:42	00:32	0:05
P4RTK	Disabled	25	372	None	4:05	17:13	1:49
P4RTK	Disabled	25		Four	4:09	19:27	1:51
P4RTK	Disabled	120	43	None	1:08	00:30	0:08
P4RTK	Disabled	120		Four	1:04	00:41	0:08

Note. Software benchmarking (hs:min) for each georeferencing scenario using three different photogrammetry software, Pix4Dmapper, OpenDroneMap, or Agisoft Metashape. Shown is the small unoccupied aircraft system (sUAS) used for the flight, whether the real-time kinematic (RTK) global positioning system was enabled or disabled, the altitude (m) above ground level, the ground control point (GCP) configuration that was used, and the total processing time for each georeferencing scenario. sUAS, small unoccupied aircraft system.

optimal performance considering the ease of implementation as well as performance across altitude and sUAS platforms. When using no GCPs or only one GCP in either the corner or middle of the field, the error was high and spatially variable across the field, which roughly corresponded to the GCP configuration used. In contrast, when four or more GCPs were used, these patterns of spatial error were diminished or disappeared entirely (Figures 6 and 7). Interestingly, geospatial error was the highest in cases where only one GCP was used rather zero GCPs. One hypothesis for why this occurred was that the use of one geotagged GCP being used for georeferencing is not enough to adequately triangulate a position and merely results in a translational shift of the imagery without appropriate scaling. When using only one GCP, distortions could be introduced due to this lack of scaling and the image set could be "pulled" to the known coordinates of the single GCP, as the image can be only be translated. The error when using one GCP was often larger than when using no GCPs, because georeferencing for the no GCP case was based on the geotagged positioning data from the metadata of each image, as recorded during the flight. Although this positioning data were less accurate than the GCP positioning data, particularly for the P4PRO and for the P4RTK with RTK disabled, it permitted georeferencing with rescaling and therefore often led to smaller georeferencing error than when using one GCP with high positioning accuracy.

Based on the results presented for sUAS not equipped with RTK, researchers that need centimeter-level georeferencing accuracy only require four GCPs placed at the corners of the study area regardless of flight altitude. This finding contrasts with those reported in Oniga et al. (2020), wherein it was found that using more GCPs could further improve results

until a plateau was reached when placing and using 20 GCPs (Oniga et al., 2020). However, that study was conducted over a ∼1 ha urban area, and thus may not directly compare with the present study, in which comparatively flat agricultural fields were the focus. Given that Oniga et al. (2020) and the present study have different visual features, this discrepancy is not surprising (Oniga et al., 2020). In the present study, the threshold reached upon using four GCPs holds true for the breeding-scale field as well as the production-scale field, which indicates that four georeferenced points should be sufficient and allow centimeter-level accuracy in many common agricultural scenarios, including at production-scale when comparing large growing areas as well as at breeding-scale when attempting to estimate specific phenotypes.

The use of the P4RTK with RTK enabled showed up to 25-fold reductions in spatial error as compared with the scenarios using the P4PRO. The accuracy of the scenarios using RTK technology did improve in some cases with the addition of GCPs, particularly regarding altitudinal accuracy; however, the 2D accuracy was sufficient in most cases without the addition of any georeferenced points. The reduction in error in the 2D plane that was observed when using GCPs with the RTK scenarios was minimal (Figures 4b and 5b). In addition, the geospatial patterns of error associated with individual GCPs that were observed in scenarios without RTK were greatly minimized or removed entirely when using the P4RTK with RTK enabled. The improvements in 3D accuracy were more substantial for these scenarios when adding even just one GCP (Figure 5b, 5d). These findings indicate that researchers that have the resources to afford and implement a sUAS equipped with RTK technology can forgo using GCPs altogether if their only concern is the accuracy of objects in the 2D plane, and

they need only use one GCP to provide centimeter-level altitudinal accuracy.

Remote sensing professionals that wish to use photogrammetry for agricultural applications require software that can perform the required tasks accurately and efficiently. As such, analysis of three popular photogrammetry software packages determined that there were key differences in their performance (Tables 3 and 4). While Pix4Dmapper and Agisoft Metashape performed most similarly of the three software regarding processing benchmarks, ODM often took much longer to process the same scenarios (Table 4). In similar fashion, the georeferencing results of the three software packages were different, with Pix4Dmapper and Metashape performing most similarly, and ODM and Metashape showing the highest number of significant differences in results (Table 3). Despite these differences in processing benchmarks and performance, it is important to note that ODM is open access, deployable from the command line, and does not have licensing fees when using the command line version, making it a viable option for professionals that want accurate results without financial input.

5 | CONCLUSIONS

When using sUAS-based photogrammetry for agricultural applications, a sufficient number and configuration of GCPs is to use four locations in the corners of the field for proper georeferencing. It is also important to note that using the entire set of GCPs in either field offered virtually no increase in accuracy along the X and Y planes and showed only minor improvements along the Z plane. For sUAS equipped with RTK, the technology can provide accurate georeferencing with error less than 7 cm without need for GCPs; however, GCPs should be used with an RTK-equipped sUAS if accuracy below 4 cm is required, such as in a breeding trial. Conversely, GCPs are likely not necessary at the production-scale when an RTK-enabled sUAS is available, because researchers and producers are often looking for differences on a larger scale and the accuracy of RTK-enabled sUAS without GCPs is likely sufficient. In summary, (a) no more than four GCPs placed at the field corners are needed for centimeter-level accuracy in the georeferencing of sUAS data at typical breeding and production scales, (b) RTK-enabled sUAS have potential for accurate data without GCPs, and (c) available software options are comparable, and choice depends on user preference and available funds.

AUTHOR CONTRIBUTIONS
N. Ace Pugh: Conceptualization; Data curation; Formal analysis; Investigation; Methodology; Software; Validation; Visualization; Writing-original draft; Writing-review & editing. Kelly R. Thorp: Conceptualization; Data curation; Formal analysis; Investigation; Methodology; Resources; Supervision; Validation; Writing-review & editing. Emmanuel M. Gonzalez: Formal analysis; Investigation; Software; Validation; Visualization; Writing-review & editing. Diaa Eldin M. Elshikha: Data curation; Investigation; Methodology; Resources; Validation; Writing-review & editing. Duke Pauli: Conceptualization; Formal analysis; Funding acquisition; Investigation; Methodology; Project administration; Resources; Supervision; Validation; Visualization; Writing-original draft; Writing-review & editing.

CONFLICTS OF INTEREST
The authors declare no conflict of interest.

ORCID
N. Ace Pugh https://orcid.org/0000-0001-7129-6556
Kelly R. Thorp https://orcid.org/0000-0001-9168-875X
Emmanuel M. Gonzalez https://orcid.org/0000-0002-3021-9842
Duke Pauli https://orcid.org/0000-0002-8292-2388

REFERENCES
Agüera-Vega, F., Carvajal-Ramírez, F., & Martínez-Carricondo, P. (2017). Assessment of photogrammetric mapping accuracy based on variation ground control points number using unmanned aerial vehicle. *Measurement: The Journal of International Measurement Confederation*, 98, 221–227. https://doi.org/10.1016/j.measurement.2016.12.002

Anderson, S. L., Murray, S. C., Malambo, L., Ratcliff, C., Popescu, S., Cope D., Chang A., Jung J., & Thomasson J. A. (2019). Prediction of maize grain yield before maturity using improved temporal height estimates of unmanned aerial systems. *The Plant Phenome Journal*, 2(1), 1–15. https://doi.org/10.2135/tppj2019.02.0004

Araus, J. L., & Cairns, J. E. (2014). Field high-throughput phenotyping: The new crop breeding frontier. *Trends in Plant Science*, 19(1), 52–61. https://doi.org/10.1016/j.tplants.2013.09.008

Borra-Serrano, I., De Swaef, T., Quataert, P., Aper, J., Saleem, A., Saeys, W., Somers B., Roldán-Ruiz, I., Lootens, P. (2020). Closing the phenotyping gap: High resolution UAV time series for soybean growth analysis provides objective data from field trials. *Remote Sensing*, 12(10), 1644. https://doi.org/10.3390/rs12101644

Colomina, I., & Molina, P. (2014). Unmanned aerial systems for photogrammetry and remote sensing: A review. *ISPRS Journal of Photogrammetry and Remote Sensing*, 92, 79–97. https://doi.org/10.1016/J.ISPRSJPRS.2014.02.013

Ekaso, D., Nex, F., & Kerle, N. (2020). Accuracy assessment of real-time kinematics (RTK) measurements on unmanned aerial vehicles (UAV) for direct geo-referencing. *Geo-spatial Information Science*, *23*(2), 165–181. https://doi.org/10.1080/10095020.2019.1710437

Fazeli, H., Samadzadegan, F., & Dadrasjavan, F. (2016). Evaluating the potential of RTK-UAV for automatic point cloud generation in 3D rapid mapping. In *The International Archives of the Photogrammetry, Remote Sensing and Spatial Information Sciences, Volume XLI-B6, 2016 XXIII ISPRS Congress, 12–19 July 2016, Prague, Czech Republic* (pp. 221–226). International Society for Photogrammetry and Remote Sensing. https://doi.org/10.5194/isprsarchives-XLI-B6-221-2016

Forlani, G., Dall'Asta, E., Diotri, F., di Cella, U. M., Roncella, R., & Santise, M. (2018). Quality assessment of DSMs produced from UAV flights georeferenced with on-board RTK positioning. *Remote Sensing*, *10*(2), 311. https://doi.org/10.3390/rs10020311

Forlani, G., Diotri, F., di Cella, U. M., & Roncella, R. (2019). Indirect UAV strip georeferencing by on-board GNSS data under poor satellite coverage. *Remote Sensing*, *11*(15), 1765. https://doi.org/10.3390/rs11151765

Gracia-Romero, A., Kefauver, S. C., Fernandez-Gallego, J. A., Vergara-Díaz, O., Nieto-Taladriz, M. T., & Araus J. L. (2019). UAV and ground image-based phenotyping: A proof of concept with durum wheat. *Remote Sensing*, *11*(10), 1244. https://doi.org/10.3390/rs11101244

Huang, Y., Brand, H. J., Sui, R., Thomson, S. J., Furukawa, T., & Ebelhar, M. W. (2016). Cotton yield estimation using very high-resolution digital images acquired with a low-cost small unmanned aerial vehicle. *Transactions of the ASABE*, *59*(6), 1563–1574. http://doi.org/10.13031/trans.59.11831

Kawamura, K., Asai, H., Yasuda, T., Khanthavong, P., Soisouvanh, P., & Phongchanmixay, S. (2020). Field phenotyping of plant height in an upland rice field in Laos using low-cost small unmanned aerial vehicles (UAVs). *Plant Production Science*, *23*(4), 452–465. https://doi.org/10.1080/1343943X.2020.1766362

Li, F., Piasecki, C., Millwood, R. J., Wolfe, B., Mazarei, M., & Stewart, C. N., Jr. (2020). High-throughput switchgrass phenotyping and biomass modeling by UAV. *Frontiers in Plant Science*, *11*. https://doi.org/10.3389/fpls.2020.574073

Malambo, L., Popescu, S. C., Murray, S. C., Putman, E., Pugh, N. A., Horne D. W., Richardson G., Sheridan R., Rooney W. L., Avant R., Vidrine M., McCutchen B., Baltensperger D., & Bishop M. (2018). Multitemporal field-based plant height estimation using 3D point clouds generated from small unmanned aerial systems high-resolution imagery. *International Journal of Applied Earth Observation and Geoinformation*, *64*, 31–42. https://doi.org/10.1016/J.JAG.2017.08.014

Martínez-Carricondo, P., Agüera-Vega, F., Carvajal-Ramírez, F., Mesas-Carrascosa, F. J., García-Ferrer, A., & Pérez-Porras, F.-J. (2018). Assessment of UAV-photogrammetric mapping accuracy based on variation of ground control points. *International Journal of Applied Earth Observation and Geoinformation*, *72*, 1–10. https://doi.org/10.1016/j.jag.2018.05.015

Merkel, D. (2014). Docker: lightweight linux containers for consistent development and deployment. *Linux Journal*, *2014*(239), 2.

Obanawa, H., Sakanoue, S., & Yagi, T. (2019). Evaluating the applicability of RTK-UAV for field management. In *International Geoscience and Remote Sensing Symposium (IGARSS)* (pp. 9090–9092). Institute of Electrical and Electronics Engineers.

Oniga, V. E., Breaban, A. I., Pfeifer, N., & Chirila, C. (2020). Determining the suitable number of ground control points for UAS images georeferencing by varying number and spatial distribution. *Remote Sensing*, *12*(5), 876. https://doi.org/10.3390/rs12050876

Pauli, D., Andrade-Sanchez, P., Carmo-Silva, A. E., Gazave, E., French, A. N., Heun, J., Hunsaker, D. J., Lipka, A. E., Setter, T. L., Strand, R. J., Thorp, K. R., Wang, S., White, J. W., & Gore, M. A. (2016). Field-based high-throughput plant phenotyping reveals the temporal patterns of quantitative trait loci associated with stress-responsive traits in cotton. G3 Genes. *Genomes, Genet*, *6*(4), 865–879. https://doi.org/10.1534/g3.115.023515

Pauli, D., Chapman, S. C., Bart, R., Topp, C. N., Lawrence-Dill, C. J., Poland, J., & Gore, M. A. (2016). The quest for understanding phenotypic variation via integrated approaches in the field environment. *Plant Physiology*, *172*(2), 622–634. https://doi.org/10.1104/pp.16.00592

Przybilla, H. J., Bäumker, M., Luhmann, T., Hastedt, H., & Eilers, M. (2020). Interaction between direct georeferencing, control point configuration and camera self-calibration for RTK-based UAV photogrammetry. *The International Archives Photogrammetry Remote Sensing and Spatial Information Sciences*, *43*(B1), 485–492. https://doi.org/10.5194/isprs-archives-XLIII-B1-2020-485-2020

Pugh, N. A., Horne, D. W., Murray, S. C., Carvalho, G., Malambo, L., Jung, J., Chang A., Maeda, M., Popescu, S., Chu, T., Starek, M. J., Brewer, M. J., Richardson, G., & Rooney, W. L. (2018). Temporal estimates of crop growth in sorghum and maize breeding enabled by unmanned aerial systems. *The Plant Phenome Journal*, *1*(1), 1–10. https://doi.org/10.2135/tppj2017.08.0006

R Development Core Team. (2011). *R: A language and environment for statistical computing*. R Core Team.

Rabah, M., Basiouny, M., Ghanem, E., & Elhadary, A. (2018). Using RTK and VRS in direct geo-referencing of the UAV imagery. *NRIAG Journal of Astronomy and Geophysics*, *7*(2), 220–226. https://doi.org/10.1016/j.nrjag.2018.05.003

Ren, H., Zhao, Y., Xiao, W., Wang, X., & Sui, T. (2020). An improved ground control point configuration for digital surface model construction in a coal waste dump using an unmanned aerial vehicle system. *Remote Sensing*, *12*(10), 1623. https://doi.org/10.3390/rs12101623

Sankaran, S., Khot, L. R., Espinoza, C. Z., Jarolmasjed, S., Sathuvalli, V. R., Vandemark, G. J., Miklas, P. N., Carter, A. H., Pumphrey, M. O., Knowles, N. R., & Pavek M. J. (2015). Low-altitude, high-resolution aerial imaging systems for row and field crop phenotyping: A review. *European Journal of Agronomy*, *70*, 112–123. https://doi.org/10.1016/J.EJA.2015.07.004

Sanz-Ablanedo, E., Chandler, J., Rodríguez-Pérez, J., & Ordóñez, C. (2018). Accuracy of unmanned aerial vehicle (UAV) and SfM photogrammetry survey as a function of the number and location of ground control points used. *Remote Sensing*, *10*(10), 1606. https://doi.org/10.3390/rs10101606

Schonberger, J. L., & Frahm, J. M. (2016). Structure-from-motion revisited. In *Proceedings of IEEE Conference on Computer Vision and Pattern Recognition, Las Vegas, 27–30 June 2016* (pp. 4104–4113). IEEE. https://doi.org/10.1109/CVPR.2016.445

Shi, Y., Thomasson, J. A., Murray, S. C., Pugh, N. A., Rooney, W. L., Shafian, S., Rajan, N., Rouze, G., Morgan, C. L. S., Neely, H. L., Rana, A., Bagavathiannan, M. V., Henrickson, J., Bowden, E., Valasek, J., Olsenholler, J., Bishop, M. P., Sheridan, R., Putman, E. B., …, Yang, C. (2016). Unmanned aerial vehicles for high-throughput

phenotyping and agronomic research. *Plos One*, *11*(7), e0159781. https://doi.org/10.1371/journal.pone.0159781

Singh, D., Wang, X., Kumar, U., Gao, L., Noor, M., Imtiaz, M., Singh, R. P., & Poland, J. (2019). High-throughput phenotyping enabled genetic dissection of crop lodging in wheat. *Frontiers of Plant Science*, *10*, 394. https://doi.org/10.3389/fpls.2019.00394

Su, W., Zhang, M., Bian, D., Liu, Z., Huang, J., Wang, W., Wu, J., & Guo, H. (2019). Phenotyping of corn plants using unmanned aerial vehicle (UAV) images. *Remote Sensing*, *11*(17), 2021. https://doi.org/10.3390/rs11172021

Taddia, Y., Stecchi, F., & Pellegrinelli, A. (2019). Using DJI Phantom 4 RTK drone for topographic mapping of coastal areas. *International Archives of the Photogrammetry, Remote Sensing and Spatial Information Sciences*, *XLII-2/W13*, 625–630. https://doi.org/10.5194/isprs-archives-XLII-2-W13-625-2019

Terpilowski, M. (2019). scikit-posthocs: Pairwise multiple comparison tests in Python. *Journal of Open Source Software*, *4*(36), 1169. https://doi.org/10.21105/joss.01169

Thorp, K., Thompson, A., Harders, S., French, A., & Ward, R. (2018). High-throughput phenotyping of crop water use efficiency via multispectral drone imagery and a daily soil water balance model. *Remote Sens*, *10*(11), 1682. https://doi.org/10.3390/rs10111682

Tonkin, T. N., & Midgley, N. G. (2016). Ground-control networks for image based surface reconstruction: An investigation of optimum survey designs using UAV derived imagery and structure-from-motion photogrammetry. *Remote Sensing*, *8*(9), 786.

Villanueva, J. K. S., & Blanco, A. C. (2019). Optimization of ground control point (GCP) configuration for unmanned aerial vehicle (UAV) survey using structure from motion (SFM). *The International Archives of the Photogrammetry Remote Sensing and Spatial Information Sciences*, *XLII-4/W12*, 167–174. https://doi.org/10.5194/isprs-archives-XLII-4-W12-167-2019

Virtanen, P., Gommers, R., Oliphant, T. E., Haberland, M., Reddy, T., Cournapeau, D., Burovski, E., Peterson, P., Weckesser, W., Bright, J., van der Walt, S. J., Brett, M., Wilson, J., Millman, K. J., Mayorov, N., Nelson, A. R. J., Jones, E., Kern, R., Larson, E., …, van Mulbregt, P. (2020). SciPy 1.0: Fundamental algorithms for scientific computing in Python. *Nature Methods*, *17*(3), 261–272. https://doi.org/10.1038/s41592-019-0686-2

Wang, J., Gea, Y., Heuvelink, G. B. M., Zhou, C., & Brus, D. (2012). Effect of the sampling design of ground control points on the geometric correction of remotely sensed imagery. *International Journal of Applied Earth Observation and Geoinformation*, *18*(1), 91–100. https://doi.org/10.1016/j.jag.2012.01.001

Westoby, M. J., Brasington, J., Glasser, N. F., Hambrey, M. J., & Reynolds, J. M. (2012). "Structure-from-motion" photogrammetry: A low-cost, effective tool for geoscience applications. *Geomorphology*, *179*, 300–314. https://doi.org/10.1016/j.geomorph.2012.08.021

Wickham, H. (2016). *ggplot2: Elegant graphics for data analysis*. Springer-Verlag. https://ggplot2.tidyverse.org

Xie, C., & Yang, C. (2020). A review on plant high-throughput phenotyping traits using UAV-based sensors. *Computers and Electronics in Agriculture*, *178*, 105731. https://doi.org/10.1016/j.compag.2020.105731

Yeom, J., Jung, J., Chang, A., Maeda, M., & Landivar, J. (2018). Automated open cotton boll detection for yield estimation using unmanned aircraft vehicle (UAV) data. *Remote Sens*, *10*(12), 1895. https://doi.org/10.3390/rs10121895

Zhou, X., Zheng, H. B., Xu, X. Q., He, J. Y., Ge, X. K., Yao, X., Cheng, T., Zhu, Y., Cao, W. X., & Tian, Y. C. (2017). Predicting grain yield in rice using multi-temporal vegetation indices from UAV-based multispectral and digital imagery. *ISPRS Journal of Photogrammetry and Remote Sensing*, *130*, 246–255. https://doi.org/10.1016/j.isprsjprs.2017.05.003

Zimmerman, T., Jansen, K., & Miller, J. (2020). Analysis of UAS flight altitude and ground control point parameters on DEM accuracy along a complex, developed coastline. *Remote Sensing*, *12*(14), 2305. https://doi.org/10.3390/rs12142305

SUPPORTING INFORMATION

Additional supporting information may be found in the online version of the article at the publisher's website.